pH-Responsive Nanostructures Assembled from Amphiphilic Block Copolymers

Chen Xu,[†] Bradford B. Wayland,[‡] Michael Fryd,[‡] Karen I. Winey,[†] and Russell J. Composto*,[†]

Department of Materials Science and Engineering and Laboratory for Research on the Structure of Matter, University of Pennsylvania, Philadelphia, Pennsylvania 19104-6272, and Department of Chemistry, University of Pennsylvania, Philadelphia, Pennsylvania 19104-6323

Received April 19, 2006; Revised Manuscript Received June 27, 2006

ABSTRACT: We present a novel route to assemble thin films containing pH-responsive nanostructures of hydrophilic cylindrical domains oriented perpendicular to a silicon substrate. The amphiphilic block copolymer, poly(styrene-*b*-acrylic acid) (PS-*b*-PAA), is prepared from the precursor, poly(styrene-*b*-*tert*-butyl acrylate) (PS-*b*-P*t*BA), by an autocatalytic reaction involving surface hydroxyl groups. The surface morphology and evolution of the nanostructures in aqueous solutions over a pH range of 2.6−9.1 are captured by in-situ atomic force microscopy (AFM). The ordered PS-*b*-PAA films exhibit unique surface morphologies across three pH regimes. At low pH (pH < 4.0) PAA chains collapse within the cylindrical domains, resulting in a hexagonal packed array of holes. At intermediate pH (4.0 < pH < 6.0) the PAA cylinders swell and transform into mushrooms with swollen caps. The height of these caps is pH-dependent, and dynamics are described by a two-stage swelling mechanism. At high pH (pH > 6.0) PAA chains stretch strongly to cover the entire surface, leading to a continuous PAA wetting layer decorated by hexagonally packed depressions. The equilibrium film thickness increases as pH increases and is reversibly recovered upon decreasing pH. The water contact angle decreases by 30° as pH increases from 2.6 to 9.1, demonstrating that wettability can be tuned by varying the pH of the surrounding medium. Because of their pH-responsive behavior and small feature size, nanostructured devices designed from amphiphilic block copolymers have potential applications including sensors and membranes.

Introduction

Soft materials that respond to external stimuli are of great interest for applications ranging from artificial muscle to drug delivery.[1−4] Polymer gels are particularly attractive as reversibly responsive materials because they can swell or collapse by several hundred times in response to subtle variations in external stimuli such as temperature, pH, and electric field.[5] Because this responsive behavior can transform chemical energy directly into mechanical work, stimuli-responsive materials can be used to build macro- or nanoscale machines such as those that mimic living organisms.[6] For example, artificial muscle and biomimetic actuators have been fabricated from polymer gels that respond to an electric field. For instance, a gel of poly(vinyl alcohol) containing free poly(acrylic acid) chains undergoes rapid bending deformation due to an applied electric field.[6] Besides bulk properties, surface properties such as wetting and biocompatibility can spontaneously adapt to environmental stimuli.[7−9] Tunable surfaces have recently been employed to create sensors, chemical gates, and protein adsorption devices.[10−14] Surface response can be imparted by structural reorganization or compositional rearrangements.[7,15] For example, layers of mixed polymer brushes or Y-shaped molecules demonstrate high sensitivity and selectivity upon exposure to good and bad solvents.[16−20]

Because they self-assemble into periodic domains with complementary properties, block copolymers are promising candidates for preparing responsive soft materials. For example, upon exposure to acetic acid, poly(styrene-*b*-methyl methacrylate) (PS-*b*-PMMA) films exhibit extensive swelling of the PMMA domains, resulting in a nanoporous structure.[21,22] Whereas a majority of copolymer studies involve hydrophobic blocks,[23−30] amphiphilic block copolymers are receiving growing interest because they can behave as nanoreactors and stimuli-responsive materials.[31] In solution, amphiphilic block copolymers self-assemble into micellar structures, such as spheres, which can be used as nanoreactors to synthesize nanoparticles or nanoclusters.[32−35] Amphiphilic block copolymers are also attractive as pH-responsive materials because domains can be tuned to respond to aqueous environments. For example, a copolymer containing a structural block that assembles into physical cross-links with a polyacid block has been used to create a chemically driven synthetic muscle.[36] Consisting of hydrophobic, glassy PMMA spheres embedded in a poly(methacrylic acid) matrix, this nanostructured gel responds in a reversible, affine manner upon exposure to cyclic pH variations. As another example, Armes et al. prepared biocompatible, pH-responsive micelles and vesicles with pH-tunable permeability.[37−39] In a novel approach to control nanostructure formation and eliminate micelle formation in solution, Krausch et al. spin-coated a triblock copolymer containing a *tert*-butyl methacrylate block which was made hydrophilic by acid-catalyzed deprotection.[40] This copolymer of poly(styrene-*b*-2-vinylpyridine-*b*-methacrylic acid) (PS-*b*-P2VP-*b*-PMAA) displayed reversible swelling/shrinking of film thickness while retaining a perforated lamella structure.

Previously, we have shown that amphiphilic diblock copolymer films of PS-*b*-PAA can self-assemble into reversible, stimuli-responsive nanostructures.[4] The nanostructure consists of perpendicular, hydrophilic, cylindrical PAA domains embedded in a glassy, hydrophobic PS matrix. Upon exposure to water,

[†] Department of Materials Science and Engineering and Laboratory for Research on the Structure of Matter.
[‡] Department of Chemistry.
* Corresponding author: phone (215) 898-4451; fax (215) 573-2128; e-mail composto@seas.upenn.edu.

10.1021/ma060881f CCC: $33.50
Published on Web 08/04/2006

the cylindrical domains swell above the surface and transform into mushroom-shaped domains. The swelling dynamics of the PAA mushrooms are captured by a two-stage mechanism, where vertical growth is described by supercase II diffusion of water into PAA followed by the slow relaxation of the PAA chains. The PS matrix is covered by the swollen PAA mushroom caps, resulting in a wettable surface. The original nanostructure is recovered upon annealing above the glass transition temperature of PAA, demonstrating the reversible nature of the swelling−shrinking process.

In the present study, we describe pH-responsive nanostructures prepared by self-assembly of amphiphilic PS-*b*-PAA. Initially, the ordered PS-*b*-PAA films contain a nearly hexagonal packed array of perpendicular PAA cylinders embedded in a continuous PS matrix. Because PAA is a weak polyelectrolyte, the film exhibits three unique nanostructured morphologies depending on pH. The surface morphology and nanostructure evolution in aqueous solutions are captured by in-situ AFM as pH increases from 2.6 to 9.1. The hexagonal packing of the PAA domains and domain spacing remain invariant upon exposure to the aqueous solutions, demonstrating that the continuous PS matrix provides mechanical stability. At intermediate pH, the swelling dynamics of the PAA mushroom cap height are described by a two-stage mechanism. Film thickness is found to increase as pH increases and is reversibly recovered upon decreasing pH. By directing the arrangement of PAA chains via pH stimulation, the water contact angle can be varied over 30°, demonstrating that amphiphilic block copolymer films can display self-adaptive surface properties.

Experimental Section

Films of PS-*b*-P*t*BA. Poly(styrene-*b*-*tert*-butyl acrylate) (PS-*b*-P*t*BA) with a polydispersity (M_w/M_n) of 1.05 was purchased from Polymer Source, Inc. The molecular weights (M_n) of the PS and P*t*BA blocks are 66 200 and 32 000 g/mol, and the volume fractions of the two blocks are $\phi_{PS} = 0.68$ and $\phi_{PtBA} = 0.32$, respectively. Prior to film deposition, silicon substrates were treated to produce surface hydroxyl groups. Silicon wafers were cleaned with a piranha solution (98% H_2SO_4/30% H_2O_2, volume ratio = 3:1) at 80 °C for 30 min. After being cooled for 30 min at room temperature, the wafers were rinsed and then immersed in ultrapure water (Millipore Direct-Q, 18.2 MΩ·cm resistivity) for 1 day. After being dried with a stream of nitrogen, substrates were exposed to UV ozone for 10 min. Thin films of PS-*b*-P*t*BA were prepared by spin-casting a 1 wt % toluene solution onto treated silicon substrates and then drying under vacuum at room temperature for 1 day. Film thickness was determined to be 40 nm using a Rudolph Research AutoEL-II Null ellipsometer with a helium−neon laser source ($\lambda = 632.8$ nm) at a fixed incident angle of 70°.

Surface Hydroxyl-Catalyzed Hydrolysis of PS-*b*-P*t*BA Films. The P*t*BA block has a thermally labile *tert*-butyl ester linkage that can be cleaved by thermal or acid-catalyzed deprotection.[4,41] Wallraff et al. demonstrated that the cleavage of the *tert*-butyl ester linkage occurs after a slow induction period followed by a fast autocatalytic process in which the deprotected groups catalyze further deprotection.[42] They also showed that acid-catalyzed deprotection occurs at a substantially reduced temperature and rapidly goes to completion. The acid-catalyzed approach has been employed to hydrolyze block copolymer films containing P*t*BMA or P*t*BA blocks using a hydrochloric acid catalyst.[40,43] Although the acidity of the surface hydroxyl groups is low, they can act as a catalyst to cleave *tert*-butyl groups at 130 °C (Scheme 1).[4,41] The low deprotection temperature (130 °C) prevents the formation of acrylic anhydride. Previously, we have demonstrated that PS-*b*-P*t*BA films with thickness values from 20 to 80 nm can be converted to amphiphilic PS-*b*-PAA films after annealing at 130 °C under vacuum for 2 days.[4] The same procedure is used in this paper. The chemical transformation from PS-*b*-P*t*BA to PS-*b*-PAA was analyzed by Fourier transform infrared spectroscopy in the attenuated total reflection mode (FTIR-ATR) (Nicolet Nexus 470 FT-IR ESP spectrophotometer configured with a Nicolet Smart DuraSampl/R ATR module). The initial film thickness (40 nm) of PS-*b*-P*t*BA, same as the thickness used for the AFM studies, was used in the FTIR-ATR analysis. To complement FTIR-ATR, the conversion of PS-*b*-P*t*BA to PS-*b*-PAA was evaluated by measuring the decrease in film thickness due to the evolution of the *tert*-butyl groups upon annealing.

Scheme 1. Chemical Transformation of PS-*b*-P*t*BA to PS-*b*-PAA by Thermal Deprotection of the *tert*-Butyl Groups Catalyzed by Surface Hydroxyl Groups

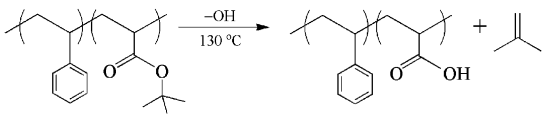

Atomic Force Microscopy (AFM) in Aqueous Environment. AFM height images were obtained using a Molecular Imaging PicoPlus scanning force microscope in the magnetic AC (MAC) mode. MAC mode is an intermittent contact mode of AFM, in which an alternating current creates an alternating magnetic field that drives the cantilever via a magnetic coating on the back of the cantilever. Silicon cantilevers with a nominal spring constant of 2.8 N/m and the tip radius of less than 7 nm were used. The resonance frequencies of the cantilevers in air and water are 75 and 30 kHz, respectively. To investigate nanostructure evolution as a function of pH, films were immersed in a liquid cell containing buffered solution and in-situ scans were performed for at least 120 min from the same area. To maintain constant counterion type and ionic strength, sodium phosphate buffers ($H_3PO_4/NaH_2PO_4/Na_2HPO_4$) were prepared with pH values ranging from 2.6 to 9.1 at fixed buffer strength (20 mM). To measure film thickness, films were scratched with a razor blade and then immersed in an aqueous medium. The height difference between the top of the film and substrate was measured by AFM. AFM images were analyzed using the grain analysis and 2D fast Fourier transform (FFT) modules from SPIP software (Image Metrology, Inc.).

Contact Angle Goniometry. Film wettability was characterized by contact angle measurements using the sessile water droplet method. Measurements were performed on a home-built static contact angle apparatus. The contact angle profiles were analyzed using Scion Image software to determine the contact angles. The contact angle values represent an average of at least 10 independent measurements.

Results and Discussion

Nanostructured Amphiphilic Block Copolymer Films of PS-*b*-PAA. The IR spectra of the initial and hydrolyzed films were recorded before (I) and after annealing at 130 °C for 2 days (II), respectively, as shown in Figure 1. Before annealing, the spectrum shows absorption bands characteristic of C=O stretching at 1725 cm^{-1}, *tert*-butyl (*t*Bu) double absorption at 1392 and 1368 cm^{-1}, and aromatic vibrations at 1491 and 1450 cm^{-1}.[4,43] After annealing, the C=O stretching vibration broadens and shifts to 1717 cm^{-1}, consistent with the formation of carboxylic acid. Second, the appearance of a broad band from ∼3300 to ∼3600 cm^{-1} is attributed to the O−H vibration in −COOH. Third, the disappearance of the two characteristic *tert*-butyl peaks at 1392 and 1368 cm^{-1} provides strong evidence for conversion to carboxylic acid.[4,40] Thus, FTIR-ATR measurements indicate that the P*t*BA block is hydrolyzed to PAA after annealing PS-*b*-P*t*BA films on a hydroxyl-rich silicon surface at 130 °C for 2 days. Furthermore, film thickness measurements of this sample support this conclusion. After annealing, film thickness decreases from 40 to 33 nm, which corresponds to a 17.5% decrease in volume. This value is in excellent agreement with the theoretical value for complete removal of the *tert*-butyl

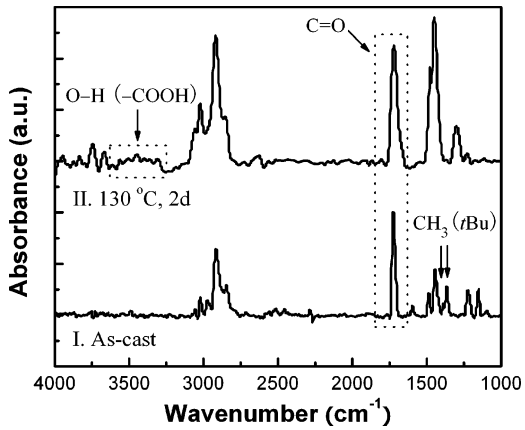

Figure 1. FTIR-ATR spectra before (I) and after (II) surface hydroxyl-catalyzed hydrolysis of a 40 nm film of PS-*b*-P*t*BA to PS-*b*-PAA.

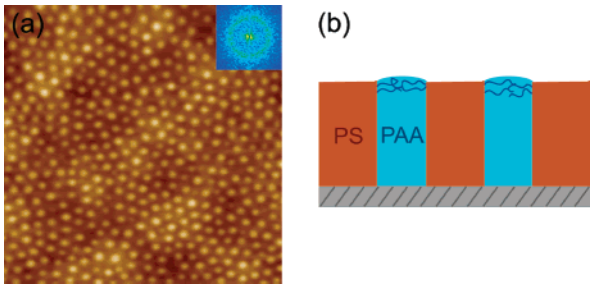

Figure 2. (a) AFM height image of a PS-*b*-PAA film (33 nm) after conversion of PS-*b*-P*t*BA by annealing at 130 °C for 2 days on a hydroxyl-rich silicon surface. The image size is 1 × 1 μm^2, and the height scale from dark to bright is 0 to 15 nm. Inset is a 2D FFT of the image. (b) Schematic cartoon of perpendicularly aligned cylindrical PAA nanodomains embedded in a PS matrix.

groups, 16.8%.[4] The chemical transformation of P*t*BA to PAA is accompanied by a change in the volume fractions of the copolymer to $\phi_{PS} = 0.81$ and $\phi_{PAA} = 0.19$.

Parts a and b of Figure 2 show the AFM height image and a schematic of the ordered PS-*b*-PAA film (thickness: 33 nm) on silicon, respectively. The AFM image was obtained at ambient conditions in air immediately after annealing. In Figure 2a, the cylindrical nanodomains of PAA (bright) are oriented normal to the substrate and organize into nearly hexagonal packing. This observation is consistent with small-angle X-ray scattering (SAXS) studies of bulk samples which display a hexagonally packed array of cylindrical PAA domains with a lattice parameter of 40.3 nm.[4] The ordering shown in Figure 2a has also been observed for film thickness values from 20 to 50 nm.[4] The average value of the cylinder diameter is 22.6 ± 2.2 nm. The inset in Figure 2a shows a 2D fast Fourier transform (FFT) of the image. The average center-to-center distance between adjacent cylinders is 49.0 nm, which is greater than the bulk value 40.3 nm.[44] The average area per cylinder is 406.0 nm^2, resulting in a PAA area fraction of 0.19, which is in outstanding agreement with the PAA volume fraction of 0.19. This consistency further supports the premise that the PAA cylinders align perpendicular to the substrate. The height difference between the cylinders and the matrix is ~2 nm and most likely results from a slight swelling of the hygroscopic PAA cylinders at ambient conditions.[40] Films of PS-*b*-PAA are of potential interest as responsive materials because the minority PAA nanodomains impart functionality whereas the majority PS provides mechanical stability. The next section investigates how amphiphilic films respond to pH variations from 2.6 to 9.1.

pH-Dependent Nanostructures of the Amphiphilic Block Copolymer Films. The pH response of the PS-*b*-PAA films is dictated by the PAA nanocylinders. Because PAA homopolymer is a weak polyelectrolyte with a pK_a 4.6,[45] the degree of ionization of the carboxylic acid groups can be tuned by varying the pH of the aqueous solution. For pH < pK_a, PAA chains collapse because the degree of ionization is rather small, and most carboxylic acid groups exist as −COOH; however, for pH > pK_a, PAA chains stretch because most acid groups are ionized.[46,47] The degree of chain stretching increases as the degree of ionization or pH increases.

Figure 3 shows AFM height images taken in sodium phosphate buffer solutions and the corresponding schematics for three regimes of pH. To ensure equilibrium morphologies, images were taken after immersion for 120 min. Longer immersion times did not result in appreciable changes in morphology. At low pH (pH < 4.0) the surface displays a nearly hexagonally packed array of holes with a characteristic hole-to-hole spacing of 50.0 nm, as shown in Figure 3a (pH 2.6) and Figure 3b (pH 3.1). Qualitatively, the PAA domains at pH 2.6 are deeper (i.e., sharper contrast) and larger than at pH 3.1. This behavior is attributed to an increase in the contraction of PAA chains as pH decreases. Quantitative cross-section analysis indicates that the average depth of holes decreases from 5.0 to 3.0 nm as pH increases from 2.6 to 3.1. Correspondingly, the average diameter of holes decreases from 22.1 and 17.3 nm, respectively. Although the diameter at pH 2.6 is similar to the initial PAA cylinder diameter (Figure 2a), the diameter at pH 3.1 is smaller than the initial value. This behavior is represented by the concave solid and dashed lines in Figure 3c, respectively. Over an intermediate pH range from near to slightly above the pK_a (4.0 < pH < 6.0), the surface is predominantly covered by a hexagonally close-packed array of mushroomlike domains, as displayed in Figure 3d,e. The average center-to-center distance between adjacent mushrooms is 51.0 nm. A similar mushroomlike nanostructure was previously observed for PS-*b*-PAA films exposed to ultrapure water (Millipore, pH = 6.0).[4] The mushroom consists of a PAA stem, surrounded by a glassy PS matrix, and a swollen PAA cap. In contrast to the circular domains under ambient conditions (Figure 2a), these caps display a planar interface because adjacent domains impinge upon each other. Correspondingly, the mushroom-shaped domains are much larger than the initial cylindrical domains. At high pH (pH > 6.0), Figure 3g,h shows that the surface displays an ordered, hexagonally packed array of depressions with an average spacing of 51.0 nm, which coincides with the original spacing of PAA cylindrical domains. The average depth of depressions is ~4.0 nm. Although the surface morphology at high pH appears similar to that at low pH (e.g., Figure 3, g and b, respectively), the surface reorganization mechanism, composition, and wettability are quite different as discussed below. Note that although the surface morphology changes significantly as pH increases from 2.6 to 8.0, the hexagonal arrangement of PAA domains and the center-to-center distance between domains are both invariant. Therefore, these findings suggest that the PS matrix imparts sufficient mechanical stability to films exposed to aqueous solutions over a range of pH.

Prior to describing the schematics in Figure 3, film thickness measurements which complement this nanostructure study will be presented. Figure 4 shows that film thickness increases as the pH increases from 2.6 to 9.1. Measurements were taken on different samples (filled squares) after immersing in aqueous solutions for ~120 min to ensure equilibrium swelling. At pH 2.6 or pH 3.1, the thickness is similar to that of the initial PS-

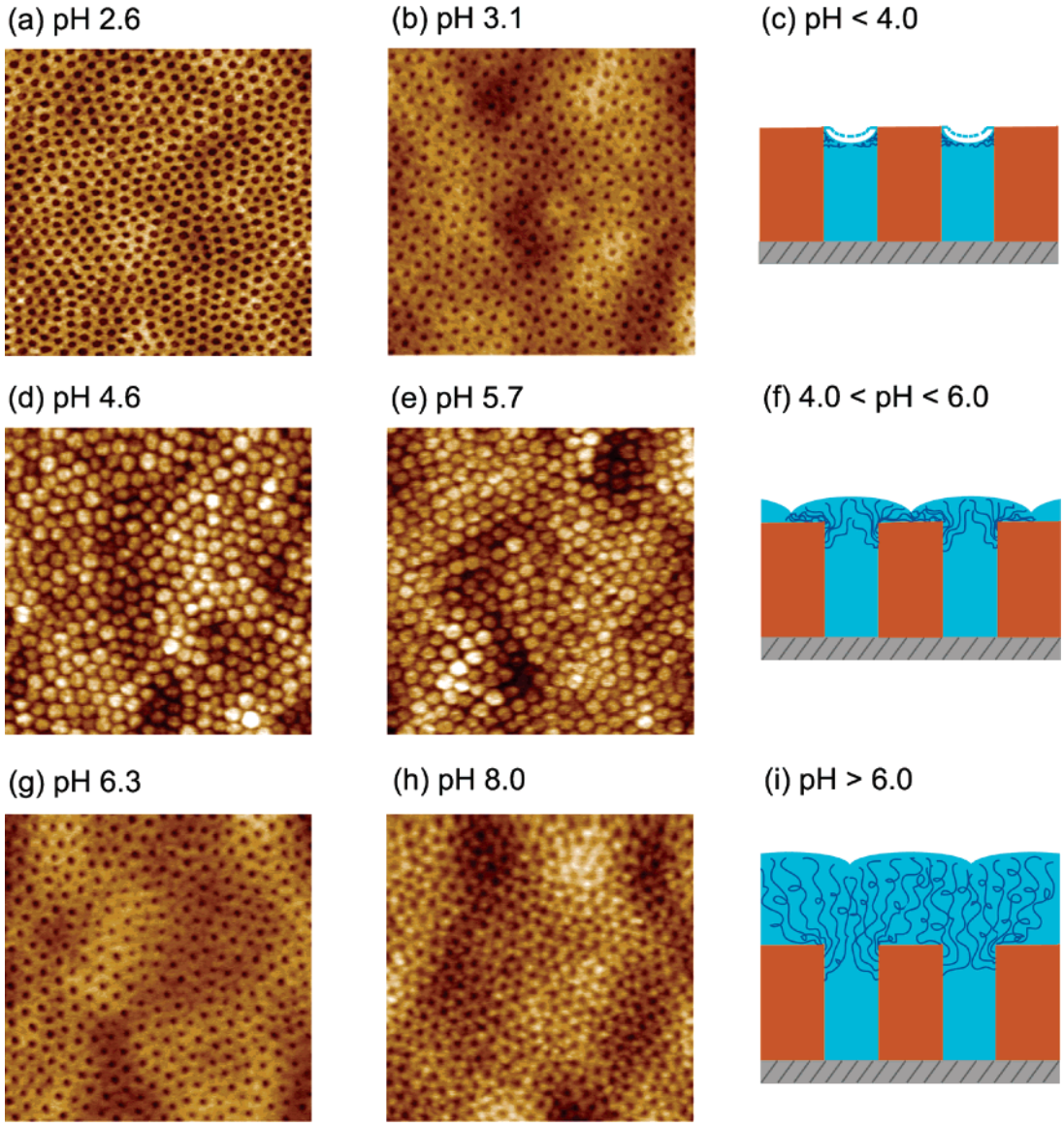

Figure 3. pH-dependent nanostructures of PS-*b*-PAA films in aqueous solutions. AFM height images of films (33 nm) immersed in buffered solutions with different pH values for ~120 min (a, b, d, e, g, h). All images are 1 × 1 μm^2, and the height scale is $\Delta z = 0-15$ nm. Schematic cartoons of cross sections at low, intermediate, and high pH regimes, where (c) pH < 4.0, (f) 4.0 < pH < 6.0, and (i) pH > 6.0, respectively. Depending on pH, PAA chains collapse or stretch, resulting in surface reconstruction of nanostructures.

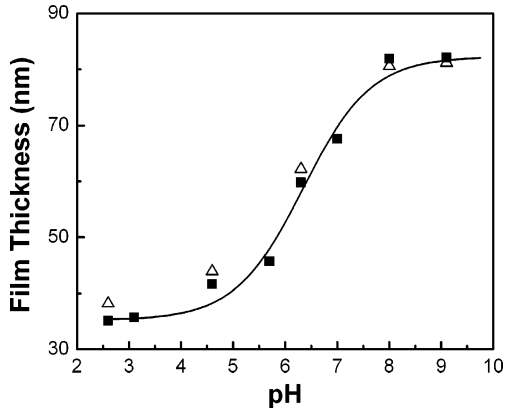

Figure 4. Film thickness in aqueous media as a function of pH. Film thickness of different samples after equilibrium swelling (filled squares). Film thickness measured from one sample as pH decreases from 9.1 to 2.6 (open triangles). The solid line is a guide to the eye. Reversible swelling is observed.

b-PAA film because PAA chains collapse within the cylindrical nanodomains, as shown in Figure 3a,b. Between pH 4.6 and pH 8.0 the film thickness increases from ~40 to ~82 nm, respectively. This behavior is consistent with stretching of PAA chains above pK_a and an increase in stretching with pH.[40,48] The stretching is driven by an increase in the number of dissociated carboxylic acid groups. A higher degree of dissociation produces a greater repulsion between carboxylate anion groups and, therefore, an increase in film thickness.[49] At pH 4.6 and pH 5.7, the total film thickness is in good agreement with the value determined by adding the PS matrix thickness and the mushroom cap height as defined below. At pH > 8.0 the film thickness levels off at a constant value of 82.0 nm. This behavior is consistent with PAA chains becoming fully dissociated at pH > 8.0,[50] which results in the maximum degree of swelling. Using the maximum thickness, the initial film thickness, and cylinder diameter under ambient conditions, a geometric argument predicts that PAA chains stretch by a maximum of ~5 times at pH > 8.0. Similar length (volume) changes have been used to build a synthetic muscle device from a block copolymer stimulated by changes in pH.[36] To test whether swelling is reversible, the film thickness of one sample

(open triangle) was monitored as pH was sequentially lowered from 9.1 to 2.6. Prior to each measurement, the film was equilibrated for 60 min. Figure 4 shows that the resulting decrease in film thickness is in excellent agreement with the swelling studies (filled squares). Thus, PS-*b*-PAA films exposed to aqueous solutions over a wide range of pH exhibit reversible swelling behavior.

We now address the schematics shown in Figure 3. With increasing pH, poly(acrylic acid) chains in solution transform from a collapsed to stretched conformation around pH = pK_a. This conformational change is induced by the electrostatic repulsion between the carboxylate ionic groups. The equilibrium chain conformation is a balance between the electrostatic interaction of the charged carboxylate anion groups, which favors stretching, and the conformational entropy of the PAA chains, which opposes stretching.[51] By considering the experimental observations that the hexagonal arrangement of the PAA domains is invariant with pH as well as the film thickness behavior with pH (Figure 4), we can construct three distinguishable nanostructures or regimes. At low pH (pH < 4.0, Figure 3c) PAA chains collapse within the cylindrical domains whereas the PS matrix remains fixed, resulting in a hexagonally packed array of holes. The dashed lines in Figure 3c represent a decrease in the contraction of PAA chains as pH increases, resulting in less chain collapse and a smaller hole diameter. At intermediate pH (4.0 < pH < 6.0, Figure 3f) PAA chains are constrained from swelling laterally by the glassy continuous PS phase and forced to stretch above the surface, leading to mushroom-shaped domains that predominantly cover the surface. In a previous study, we proposed a model to describe the formation of such mushrooms.[4] As they absorb water, the PAA domains, confined by the glassy PS matrix, can only swell vertically above the surface and horizontally along the surface. PAA chains near the surface of the cylinders extend laterally across the PS matrix, whereas PAA chains below the surface extend toward the apex of the caps. At high pH (pH > 6.0, Figure 3i) PAA chains are highly stretched and occupy the entire surface. Although the low and high pH regimes appear to display similar surface morphologies, their surface features result from different surface reconstruction pathways. Namely, at high pH, the junction between PS and PAA is bound to the intermaterial dividing surface (IMDS), and PAA chains below the surface can stretch only vertically (i.e., junction point does not diffuse toward solution). Thus, at a high degree of chain stretching, the depressions overlying the cylinders result from an inability of PAA chains from deep beneath the surface to extend out into solution as much as PAA chains with junction points closer to the surface. The cross sections corresponding to low, intermediate, and high pH regimes (Figure 3c,f,i) will be further supported by in-situ AFM and surface wettability measurements in the following sections.

In-Situ AFM and Swelling Dynamics. In-situ AFM was performed to observe the evolution of the nanostructures and the swelling dynamics of PS-*b*-PAA films in aqueous solutions with different pH values. Scans from the same region were taken every ~5 min for a total of ~120 min. Figure 5a was obtained immediately after sample immersion (pH 4.6) and microscope alignment. After 17 min, the PAA domain diameter is already much larger than in the initial state (Figure 2a) and continues to increase until adjacent domains impinge after 33 min (Figure 5b). Vertically, dimples about 2 nm deep develop in the center of PAA domains after 17 min, as shown in Figure 5a. The growth in the lateral and vertical directions is consistent with a rapid relaxation of PAA chains near the surface followed by a slower relaxation of PAA chains from below the surface, respectively. However, comparison of Figure 5a,b shows that the dimples disappear after 33 min of immersion, and the domain height increases significantly as denoted by the greater contrast in Figure 5b relative to Figure 5a. Similar swelling behavior has also been observed at pH 5.7, except that the dynamics are faster as discussed below. Figure 5c displays a cartoon of a PAA mushroom with cap diameter (*D*) and cap height (*H*). Being confined by the continuous glassy PS matrix, the stem of PAA is unable to swell laterally and, thus, has a limited capacity to take up water. This interpretation is consistent with the invariance of the PAA domain separation and the hexagonal packing observed for initial and wet films. Because of matrix confinement, the PAA nanodomains can only absorb water by swelling vertically above the surface and horizontally along the surface, resulting in the mushroom-shaped domains described by Figure 5c. To form the cap, PAA chains near the surface of the cylinders extend laterally across the PS matrix to form the base of the cap whereas PAA chains below the surface extend toward the apex to form the hemispherical cap. Figure 5d displays the distribution of PAA domain diameters before (cylinder) and after (mushroom) swelling. Upon swelling, *D*, as defined by the Gaussian maximum, increases by more than 2 times, from 22.6 ± 2.2 to 49.3 ± 6.5 nm. The *D* after swelling is also approximately equal to the cylinder−cylinder spacing in the initial film (Figure 2a), consistent with the premise that caps swell to cover the entire surface. The histogram also shows that the distribution of *D* broadens upon swelling. While the increase in *D* occurs rapidly, the vertical swelling of the caps is much slower as described next.

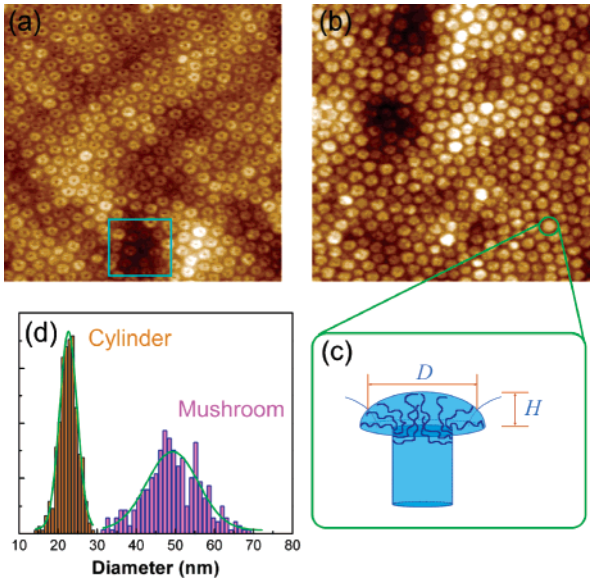

Figure 5. AFM height images of nanostructured films of PS-*b*-PAA after swelling at pH 4.6 for 17 min (a) and 33 min (b). Both images are 1 × 1 μm^2, and the height scale is $\Delta z = 0-15$ nm. (c) Schematic illustration of the mushroomlike nanostructure having a stem and cap of diameter *D* and height *H*. The cap forms as water diffuses into the PAA domain and PAA chains stretch out of the stem to form a water-swollen cap. (d) Histogram of diameters for the initial cylinders (Figure 2a) and the swollen mushroom at pH 4.6.

The height of the swollen cap *H* is defined as the difference between the apex of the mushroom and the surface of the PS matrix. To accurately determine the swollen cap height, *H* was measured near defects (e.g., the box in Figure 5a) where the PS matrix is exposed. Figure 6 shows the cap height *H* as a function of time at pH 4.6 and pH 5.7. Qualitatively, in either aqueous solution, the growth of *H* consists of an early stage,

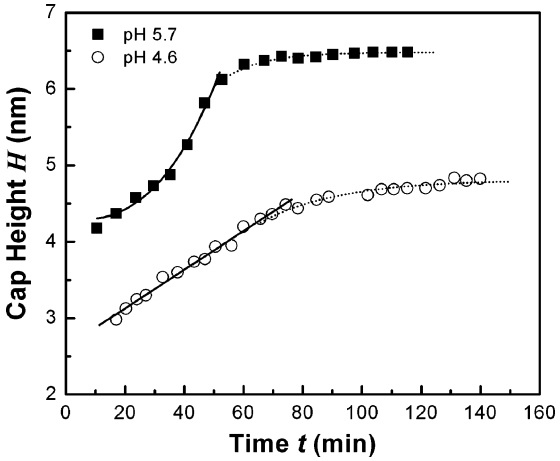

Figure 6. Swelling dynamics of the PAA mushroom cap height H at pH 4.6 and pH 5.7. The solid and dotted lines are fits to the data using eqs 1 and 2, respectively.

where H grows rapidly, and a late stage, where H grows more slowly and approaches its maximum value. At pH 4.6, H steadily grows from 3.0 to 4.4 nm between 17 and 70 min, respectively. After 70 min, H slowly approaches the maximum height of 4.8 nm. However, films immersed in solution with pH 5.7 swell more rapidly than at the lower pH. At pH 5.7 H grows quickly from 4.2 to 6.1 nm between 10 and 53 min, respectively. After 53 min, H grows more slowly and approaches a maximum value of 6.5 nm. The swelling dynamics of the PAA caps are consistent with the two-stage process described below.

To understand nanostructure swelling, we apply a two-stage model previously used to describe the swelling dynamics of nanostructured PS-*b*-PAA films and weak polyelectrolyte films.[4,52] The dynamics are initially governed by diffusion of a penetrant into the polymer and then by a slow relaxation of the polymer chains. In the case of PAA mushrooms, the initial growth of the cap height due to water diffusion into PAA is described by

$$\frac{H}{H_\infty} = A + k_1 t^n \tag{1}$$

where H_∞ is the cap height at equilibrium, A is equal to the initial cap height normalized by H_∞, k_1 is a rate constant that depends on the local environment of the penetrant, and n is the scaling exponent that depends on the diffusion mechanism. For $n = 0.5$, $0.5 < n < 1.0$, $n = 1.0$, or $n > 1.0$, diffusion is described as Fickian, anomalous, case II, or supercase II, respectively. At high volume fractions of water, swelling becomes dominated by molecular relaxation and is described by

$$\frac{H}{H_\infty} = 1 - B\exp(-k_2 t) \tag{2}$$

where B is a scaling constant and k_2 reflects the rate of chain relaxation. Figure 6 clearly shows that the swelling dynamics are pH-dependent. At pH 4.6, H during the initial stage was fit with eq 1 using $n = 1$ (solid line), suggesting that water diffusion into the PAA nanodomains follows the case II mechanism. However, at pH 5.7 accelerated growth is observed and eq 1 was fit to H values using $n = 2.68$ (solid line), suggesting that water diffusion into the PAA nanodomains follows supercase II. Case II and supercase II diffusion have been reported for PAA multilayers in aqueous solution.[52] Moreover, PS-*b*-PAA films have been observed to exhibit supercase II diffusion ($n = 2.64$) when swollen in ultrapure water at pH = 6.0.[4] The dependence of the swelling dynamics on pH is related to the degree of ionization of the weak polyelectrolyte PAA. As the fraction of ionized acrylic acid groups increases with increasing pH (pH 5.7 > pH 4.6), the electrostatic repulsion between the carboxylate ionic groups in the PAA nanodomains is expected to increase. Therefore, the PAA domains in a higher pH solution should exhibit an enhanced water permeation rate as experimentally observed. The second stage of growth attributed to polymer relaxation also appears to be pH-dependent, as shown in Figure 6. Namely, the relaxation of PAA chains at pH 5.7 is faster than at pH 4.6. The dotted lines in Figure 6 were fit using $k_2 = 0.04$ and $0.08\ \text{min}^{-1}$ for pH 4.6 and 5.7, respectively, corresponding to characteristic relaxation times of 1500 and 750 s.

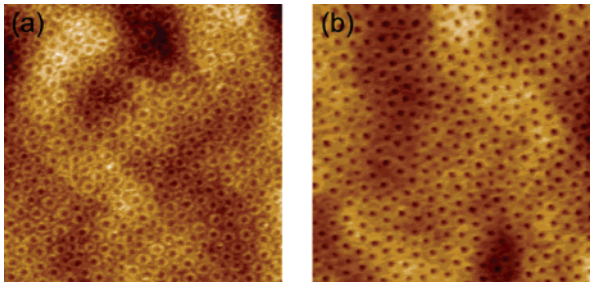

Figure 7. Evolution of nanostructures at high pH (pH > 6.0). AFM height images of PS-*b*-PAA films after swelling at pH 6.3 for 18 min (a) and 30 min (b). The depressions are 2.0 and 3.0 nm deep in (a) and (b), respectively. Both images are $1 \times 1\ \mu\text{m}^2$, and the height scale is $\Delta z = 0-15$ nm.

Although the surface features at low and high pH appear to be similar (e.g., compare parts b and g of Figure 3), film thickness measurements suggest that these regimes display significantly different reconstruction pathways and surface composition. To further distinguish these regimes, the evolution of the nanostructures at both low and high pH was investigated via in-situ AFM. At low pH (2.6 or 3.1) the surface developed hexagonally packed holes immediately after immersion (data not shown). Continuous scanning for about 120 min revealed that these surface holes did not change with time. In contrast, for pH > 6.0 the nanostructured surface evolved significantly with time. Figure 7 is a representative example of nanostructure evolution at high pH. After swelling at pH 6.3 for 18 min, the surface of PS-*b*-PAA films displays donut-shaped features as shown in Figure 7a. Similar features are observed at intermediate pH values as well. This similarity suggests that the swelling mechanism at high pH is the same as that observed for the mushroom caps at intermediate pH, except that the degree of swelling and the swelling dynamics differ. As discussed previously, PAA chains near the top of the stem extend laterally across the PS matrix, whereas PAA chains below the surface stretch toward the center of the PAA domains (Figure 3f,i). Because swelling is less at intermediate pH, the chains below the surface are able to reach the apex of the cap. However, at high pH, these chains are unable to stretch enough to maintain a hemispherical shape. The surface depression at high pH can be shown to differ from that at low pH by investigating the nanostructure evolution. After swelling at pH 6.3 for 30 min, Figure 7b shows that the rims around PAA domains merge with adjacent domains to produce a continuous PAA surface with depressions situated directly over the center of the initial cylinders. Comparison of images after 30 min (Figure 7b) and 120 min (Figure 3g) reveals no appreciable difference, indicating that swelling of the nanostructured PS-*b*-PAA films at pH 6.3 reaches equilibrium in ~30 min. Indeed, film thickness mea-

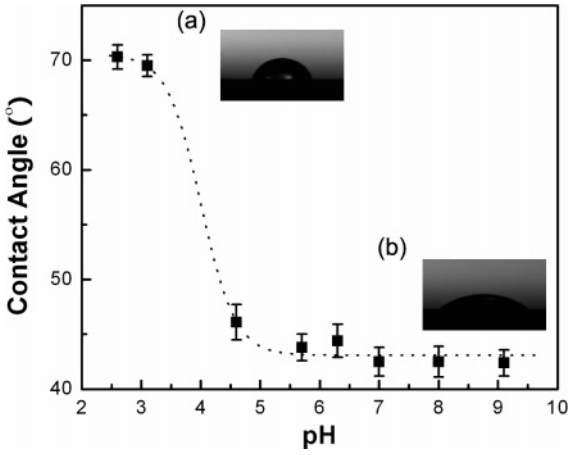

Figure 8. Water contact angles on dried PS-*b*-PAA films after initial immersion at different pH values. The dotted line is a guide to the eye. Inset (a) represents a typical droplet profile at pH < 4.0 (e.g., pH 2.6), whereas inset (b) is a representative profile at pH > 4.0 (e.g., pH 8.0). The ~30°decrease in contact angle is attributed to surface rearrangement of PAA chains.

surements at high pH are found to reach their equilibrium value within 20−30 min.

Tunable Surface Properties. Film wettability can be regulated by varying the surface composition of films. The measured water contact angle for the initial PS-*b*-PAA films is 73°, very close to the value (77°) determined from the Cassie−Baxter equation using an area fraction of 81% PS (19% PAA) at the surface.[18] In this study, PS-*b*-PAA films immersed in aqueous solutions of varying pH values are found to undergo dramatic surface rearrangement and changes in surface composition, as shown in Figure 3. The tunable wetting properties can be monitored by measuring the water contact angles on PS-*b*-PAA films after exposure to pH buffered solutions for 120 min. By rapidly drying samples prior to contact angle measurements, the surface morphology was preserved as confirmed by AFM. Figure 8 shows that the contact angle decreases abruptly as pH increases. Inset (a) displays a profile of a typical droplet at pH 2.6 or pH 3.1. The contact angle of ~70° is similar to that of the initial PS-*b*-PAA film, 73°, indicating that the surface compositions are similar. Therefore, at low pH, the contact angle measurements are consistent with AFM analysis, which suggests that PAA chains collapse within the initial cylindrical domains (i.e., Figure 3c). However, as pH increases, the contact angle value decreases abruptly as pH 4.0 is approached and then reaches a constant value of ~43° above pH 5.0. Inset (b) shows a typical droplet profile on a surface prepared at pH > 4.0. The decrease in contact angle is attributed to the conformational rearrangement of PAA chains in response to the high pH environment, resulting in a more hydrophilic surface. The contact angles (~43°) at pH > 4.0 are very similar to the values for grafted PAA brushes (~42°),[53−55] suggesting that the entire surface is covered by PAA. Indeed, AFM measurements indicate that the surface is predominantly covered by PAA mushrooms at pH 4.6 and pH 5.7 and entirely covered by PAA chains at pH > 6.0. The hydrophilicity of the surface increases dramatically as indicated by a significant decrease in contact angle, ~30°. This enhancement in wettability is attributed to the self-adaptive surface property of the amphiphilic block copolymer films investigated here.

Conclusions

In conclusion, we have demonstrated a novel route to fabricate pH-responsive nanostructures via an autocatalytic reaction, where the amphiphilic block copolymer PS-*b*-PAA is transformed from PS-*b*-P*t*BA by thermal deprotection of the *tert*-butyl groups catalyzed by surface hydroxyl groups on silicon substrates. The resulting amphiphilic block copolymer films self-assemble into a nearly hexagonal packed array of perpendicular PAA cylinders surrounded by a continuous PS matrix. Because PAA is a weak polyelectrolyte, the film exhibits different nanostructures depending on the pH regime. At low pH (pH < 4.0) PAA chains collapse within the cylindrical domains, leading to a hexagonal packed array of holes embedded in the PS matrix. At intermediate pH (4.0 < pH < 6.0) PAA swells and the cylindrical domains transform into mushrooms with a swollen cap, which predominantly cover the surface. At high pH (pH > 6.0) PAA chains stretch considerably to cover the entire surface, resulting in a continuous PAA phase with hexagonally packed depressions on top of the initial cylinders. The overall hexagonal packing of the PAA domains remains unchanged upon exposure to the aqueous solutions, implying that the continuous PS matrix provides mechanical stability. This stability is the key to the reversible nature of the swollen nanostructures. Because the PAA chains swell above the original surface, the film thickness increases as pH increases and reaches a maximum value at pH > 8.0. The film thickness is recovered upon decreasing pH, demonstrating the reversibility of the swelling process. The evolution of these nanostructures and the swelling dynamics of the PAA mushrooms are captured by in-situ AFM. The swelling dynamics of the cap height depend on pH and are described by a two-stage mechanism, where initial growth is controlled by case II (pH 4.6) or supercase II (pH 5.7) diffusion of water into PAA domains followed by the slow relaxation of the PAA chains. Furthermore, contact angle measurements indicate that wettability can be regulated by controlling the conformational rearrangement of PAA chains in response to a pH stimulus. We anticipate that this study will provide motivation for the design of new self-assembled, nanoscale devices that exhibit pH-responsive behavior.

Acknowledgment. This work was financially supported by grants from NSF/MRSEC (DMR05-20020), NSF/Polymer Program (DMR02-34903), NSF/NSEC (DMR04-25780), and NSF (CHE05-01198). Acknowledgment is made to the donors of the American Chemical Society Petroleum Research Fund for partial support of this research. C.X. thanks Mark H. Lee and Xuefeng Fu for helpful discussions. We thank MI/Agilent for assistance with optimizing in-situ studies using the PicoPlus AFM.

References and Notes

(1) Minko, S.; Muller, M.; Usov, D.; Scholl, A.; Froeck, C.; Stamm, M. *Phys. Rev. Lett.* **2002**, *88*, 035502.
(2) Nath, N.; Chilkoti, A. *Adv. Mater.* **2002**, *14*, 1243−1247.
(3) Russell, T. P. *Science* **2002**, *297*, 964−967.
(4) Xu, C.; Fu, X. F.; Fryd, M.; Xu, S.; Wayland, B. B.; Winey, K. I.; Composto, R. J. *Nano Lett.* **2006**, *6*, 282−287.
(5) Tanaka, T.; Nishio, I.; Sun, S. T.; Uenonishio, S. *Science* **1982**, *218*, 467−469.
(6) Galaev, I. Y.; Mattiasson, B. *Trends Biotechnol.* **1999**, *17*, 335−340.
(7) Crowe, J. A.; Genzer, J. *J. Am. Chem. Soc.* **2005**, *127*, 17610−17611.
(8) Efimenko, K.; Crowe, J. A.; Manias, E.; Schwark, D. W.; Fischer, D. A.; Genzer, J. *Polymer* **2005**, *46*, 9329−9341.
(9) Minko, S.; Muller, M.; Motornov, M.; Nitschke, M.; Grundke, K.; Stamm, M. *J. Am. Chem. Soc.* **2003**, *125*, 3896−3900.
(10) Gillies, E. R.; Jonsson, T. B.; Frechet, J. M. J. *J. Am. Chem. Soc.* **2004**, *126*, 11936−11943.
(11) Huber, D. L.; Manginell, R. P.; Samara, M. A.; Kim, B. I.; Bunker, B. C. *Science* **2003**, *301*, 352−354.
(12) Ito, Y.; Ochiai, Y.; Park, Y. S.; Imanishi, Y. *J. Am. Chem. Soc.* **1997**, *119*, 1619−1623.
(13) Park, M. K.; Deng, S. X.; Advincula, R. C. *J. Am. Chem. Soc.* **2004**, *126*, 13723−13731.

(14) Tokareva, I.; Minko, S.; Fendler, J. H.; Hutter, E. *J. Am. Chem. Soc.* **2004**, *126*, 15950−15951.
(15) Zhang, W. Q.; Shi, L. Q.; Ma, R. J.; An, Y. L.; Xu, Y. L.; Wu, K. *Macromolecules* **2005**, *38*, 8850−8852.
(16) Gorodyska, G.; Kiriy, A.; Minko, S.; Tsitsilianis, C.; Stamm, M. *Nano Lett.* **2003**, *3*, 365−368.
(17) Julthongpiput, D.; Lin, Y. H.; Teng, J.; Zubarev, E. R.; Tsukruk, V. V. *Langmuir* **2003**, *19*, 7832−7836.
(18) Julthongpiput, D.; Lin, Y. H.; Teng, J.; Zubarev, E. R.; Tsukruk, V. V. *J. Am. Chem. Soc.* **2003**, *125*, 15912−15921.
(19) Kiriy, A.; Gorodyska, G.; Minko, S.; Stamm, M.; Tsitsilianis, C. *Macromolecules* **2003**, *36*, 8704−8711.
(20) Lupitskyy, R.; Roiter, Y.; Tsitsilianis, C.; Minko, S. *Langmuir* **2005**, *21*, 8591−8593.
(21) Xu, T.; Stevens, J.; Villa, J. A.; Goldbach, J. T.; Guarim, K. W.; Black, C. T.; Hawker, C. J.; Russell, T. R. *Adv. Funct. Mater.* **2003**, *13*, 698−702.
(22) Xu, T.; Goldbach, J. T.; Misner, M. J.; Kim, S.; Gibaud, A.; Gang, O.; Ocko, B.; Guarini, K. W.; Black, C. T.; Hawker, C. J.; Russell, T. P. *Macromolecules* **2004**, *37*, 2972−2977.
(23) Bates, F. S.; Fredrickson, G. H. *Annu. Rev. Phys. Chem.* **1990**, *41*, 525−557.
(24) Bockstaller, M. R.; Mickiewicz, R. A.; Thomas, E. L. *Adv. Mater.* **2005**, *17*, 1331−1349.
(25) Hammond, M. R.; Cochran, E.; Fredrickson, G. H.; Kramer, E. J. *Macromolecules* **2005**, *38*, 6575−6585.
(26) Hobbs, J. K.; Register, R. A. *Macromolecules* **2006**, *39*, 703−710.
(27) Park, C.; Yoon, J.; Thomas, E. L. *Polymer* **2003**, *44*, 6725−6760.
(28) Park, M. J.; Char, K.; Bang, J.; Lodge, T. P. *Macromolecules* **2005**, *38*, 2449−2459.
(29) Segalman, R. A.; Hexemer, A.; Hayward, R. C.; Kramer, E. J. *Macromolecules* **2003**, *36*, 3272−3288.
(30) Xiang, H. Q.; Lin, Y.; Russell, T. P. *Macromolecules* **2004**, *37*, 5358−5363.
(31) Forster, S.; Antonietti, M. *Adv. Mater.* **1998**, *10*, 195−217.
(32) Aizawa, M.; Buriak, J. M. *J. Am. Chem. Soc.* **2006**, *128*, 5877−5886.
(33) Bennett, R. D.; Miller, A. C.; Kohen, N. T.; Hammond, P. T.; Irvine, D. J.; Cohen, R. E. *Macromolecules* **2005**, *38*, 10728−10735.
(34) Boontongkong, Y.; Cohen, R. E. *Macromolecules* **2002**, *35*, 3647−3652.
(35) Rodriguez-Hernandez, J.; Lecommandoux, S. *J. Am. Chem. Soc.* **2005**, *127*, 2026−2027.
(36) Howse, J. R.; Topham, P.; Crook, C. J.; Gleeson, A. J.; Bras, W.; Jones, R. A. L.; Ryan, A. J. *Nano Lett.* **2006**, *6*, 73−77.
(37) Du, J. Z.; Armes, S. P. *J. Am. Chem. Soc.* **2005**, *127*, 12800−12801.
(38) Du, J. Z.; Tang, Y. P.; Lewis, A. L.; Armes, S. P. *J. Am. Chem. Soc.* **2005**, *127*, 17982−17983.
(39) Liu, S. Y.; Weaver, J. V. M.; Tang, Y. Q.; Billingham, N. C.; Armes, S. P.; Tribe, K. *Macromolecules* **2002**, *35*, 6121−6131.
(40) Ludwigs, S.; Schmidt, K.; Krausch, G. *Macromolecules* **2005**, *38*, 2376−2382.
(41) La, Y. H.; Edwards, E. W.; Park, S. M.; Nealey, P. F. *Nano Lett.* **2005**, *5*, 1379−1384.
(42) Wallraff, G.; Hutchinson, J.; Hinsberg, W.; Houle, F.; Seidel, P.; Johnson, R.; Oldham, W. *J. Vac. Sci. Technol., B: Microelectron., Process., Phenom.* **1994**, *12*, 3857−3862.
(43) Feng, C. L.; Vancso, G. J.; Schonherr, H. *Langmuir* **2005**, *21*, 2356−2363.
(44) Kim, S. H.; Misner, M. J.; Xu, T.; Kimura, M.; Russell, T. P. *Adv. Mater.* **2004**, *16*, 226−231.
(45) Dautzenberg, H.; Jaeger, W.; Kotz, J.; Philipp, B.; Seidel, Ch.; Stscherbina, D. *Polyelectrolytes: Formation, Characterization and Application*; Hanser: New York, 1994.
(46) Schilli, C. M.; Zhang, M. F.; Rizzardo, E.; Thang, S. H.; Chong, Y. K.; Edwards, K.; Karlsson, G.; Muller, A. H. E. *Macromolecules* **2004**, *37*, 7861−7866.
(47) Sonnenberg, L.; Parvole, J.; Borisov, O.; Billon, L.; Gaub, H. E.; Seitz, M. *Macromolecules* **2006**, *39*, 281−288.
(48) Kozlovskaya, V.; Kharlampieva, E.; Mansfield, M. L.; Sukhishvili, S. A. *Chem. Mater.* **2006**, *18*, 328−336.
(49) Biesalski, M.; Johannsmann, D.; Ruhe, J. *J. Chem. Phys.* **2002**, *117*, 4988−4994.
(50) Guo, X.; Ballauff, M. *Langmuir* **2000**, *16*, 8719−8726.
(51) Currie, E. P. K.; Sieval, A. B.; Fleer, G. J.; Stuart, M. A. C. *Langmuir* **2000**, *16*, 8324−8333.
(52) Tanchak, O. M.; Barrett, C. J. *Chem. Mater.* **2004**, *16*, 2734−2739.
(53) Treat, N. D.; Ayres, N.; Boyes, S. G.; Brittain, W. J. *Macromolecules* **2006**, *39*, 26−29.
(54) Janorkar, A. V.; Metters, A. T.; Hirt, D. E. *Macromolecules* **2004**, *37*, 9151−9159.
(55) Li, J.; Chen, X. R.; Chang, Y. C. *Langmuir* **2005**, *21*, 9562−9567.

MA060881F